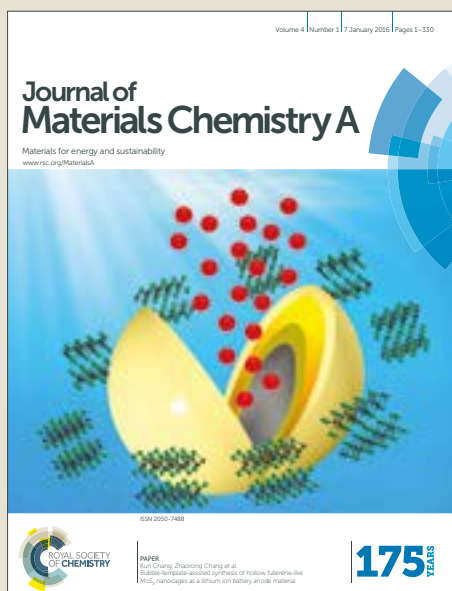


Journal of Materials Chemistry A

Accepted Manuscript



This article can be cited before page numbers have been issued, to do this please use: H. K. Kim, C. Lu, I. Choi and J. Kim, *J. Mater. Chem. A*, 2017, DOI: 10.1039/C7TA04762B.



This is an Accepted Manuscript, which has been through the Royal Society of Chemistry peer review process and has been accepted for publication.

Accepted Manuscripts are published online shortly after acceptance, before technical editing, formatting and proof reading. Using this free service, authors can make their results available to the community, in citable form, before we publish the edited article. We will replace this Accepted Manuscript with the edited and formatted Advance Article as soon as it is available.

You can find more information about Accepted Manuscripts in the [author guidelines](#).

Please note that technical editing may introduce minor changes to the text and/or graphics, which may alter content. The journal's standard [Terms & Conditions](#) and the ethical guidelines, outlined in our [author and reviewer resource centre](#), still apply. In no event shall the Royal Society of Chemistry be held responsible for any errors or omissions in this Accepted Manuscript or any consequences arising from the use of any information it contains.

Simple Synthesis and Molecular Engineering of Low-cost and Star-shaped Carbazole-based Hole Transporting Materials for Highly Efficient Perovskite Solar Cells

Chunyuan Lu^{a†}, In Taek Choi^{a†}, Jeongho Kim^b and Hwan Kyu Kim^{a,*}

^aGlobal GET-Future Lab. and Department of Advanced Materials Chemistry, Korea University, Sejong 300-79, Korea

^bDepartment of Chemistry, Inha University, 100 Inha-ro, Incheon 402-751, Korea

*To whom correspondence should be addressed: Email: hkk777@korea.ac.kr

[†]These authors equally contributed to this work.

Electronic supplementary information (ESI) available. See DOI:

Abstract

Perovskite solar cells (PrSCs) have emerged as a very promising technology in the field of photovoltaics by demonstrating power conversion efficiencies (PCEs) soaring from 3.9% to above 22% within the past eight years. To date, perovskite solar cells mainly depend on *spiro-OMeTAD* to perform a key role as a hole transporting material (HTM). However, the complicated multi-step synthetic procedures and high-cost purification process for *spiro-OMeTAD* limited its potential for commercial application. Herein, three new carbazole-based HTMs with starburst structure, coded as **SGT-405(3,6)**, **SGT-410(3,6)** and **SGT-411(3,6)** via tuning the substitution position from (2,7) to (3,6) position of carbazole moiety, have been successfully synthesized via three-step synthesis from commercial available reagents and investigated for highly efficient perovskite solar cells. By adopting this strategy, among them, molecularly engineered carbazole derivative **SGT-405(3,6)** exhibits significantly increased T_g (192.7°C), improved film forming ability, reduced hole reorganization energy and enhanced hole mobility compared to its parent molecule **SGT-405(2,7)** and *spiro-OMeTAD*. Owing to the promising properties of **SGT-405(3,6)**, meso-porous type PrSCs employing **SGT-405(3,6)** showed a remarkable PCE of 18.87%, which is better than the photovoltaic device employing *spiro-OMeTAD* (17.71%). To the best of our knowledge, the achieved PCE (18.87%) is the highest value reported for devices with the structure of FTO/compact TiO₂/meso-porous TiO₂/CH₃NH₃PbI_{3-x}Cl_x/HTM/Au employing small-molecular HTMs. Meanwhile, owing to the simple synthesis of **SGT-405(3,6)**, compared with **SGT-405(2,7)** previously developed by our group, synthesis cost was much lowered, resulting in low cost compared to the *spiro-OMeTAD* and **SGT-405(3,6)**, by approximately three times. Furthermore, the long-term device stability of PrSCs was enhanced for **SGT-405(3,6)** to some extent compared to other HTMs studied here due to the good uniform capping layer of **SGT-405(3,6)** on top of perovskite layer and the prevention of the moisture penetration into the perovskite layer. Therefore, **SGT-405(3,6)** is a promising low-cost and effective non-spiro type HTM with potential to replace expensive *spiro-OMeTAD* for PrSCs.

Key words: hole-transporting materials, carbazole, simple synthesis, hole mobility, film forming ability, perovskite solar cells

Introduction

Perovskites have been widely employed as efficient light absorbing layer for photovoltaic cells due to their broad spectral absorption^{1,2} from visible to near-infrared, high charge carrier mobilities,³ long charge diffusion lengths,^{4,5} small exciton binding energy (ca. 50 meV),⁶ solution-processing abilities.⁷ Very recently, the certified power conversion efficiency (PCE) of perovskite solar cells has skyrocketed to over 22%.⁸ Due to the rapid development of perovskite solar cells (PrSCs), it was elected as one of the top ten emerging technologies of 2016.⁹

Hole-transporting material (HTM) is a necessary component¹⁰ for efficient PrSCs, since HTMs play a critical role in efficiently extracting holes from perovskite to HTM layer and simultaneously transmitting to counter electrode in order to decrease in charge recombination and loss of V_{oc} . So far, *spiro-OMeTAD* is still the most commonly used hole transporting material for efficient PrSCs. Unfortunately, complicated synthetic scheme and high-cost purification procedures (sublimation) for *spiro-OMeTAD* result in efficient but costly materials, because the synthesis of *spiro-OMeTAD* involved five reaction steps that require low temperature (-78°C), and sensitive (n-butyl-lithium or Grignard reagents) and aggressive (Br_2) reagents.¹¹ In addition, the purities in HTMs can act as trap site for holes, thus high-purity sublimation-grade *spiro-OMeTAD* is required to obtain high-performance devices.¹² The complicated synthesis and high-cost purification procedures (sublimation) of *spiro-OMeTAD* hindered its potential for commercialization of efficient PrSCs. Therefore it is necessary to develop more economical and efficient alternative non-spiro type HTMs to *spiro-OMeTAD*.

Carbazole derivatives have attracted much attention due to their interesting photochemical properties.^{13,14} Increased attention on carbazole-based derivatives could be explained by the features of carbazole derivatives's: low cost of the 9H-carbazole starting material, good chemical and environmental stability, versatility of the carbazole reactive sites that can react with a wide variety of functional groups to fine tuning of its electronic and optical properties.¹⁵⁻¹⁷ In our previous work, we reported the synthesis and characterization of carbazole-based HTMs with two- or three-arm chemical structures, which were linked through phenylene-derived central core units. We also investigated their application in $CH_3NH_3PbX_3$ -based perovskite-sensitized solar cells.^{18,19}

In this work, in order to further decrease the synthesis cost and improve the hole transporting capability, we designed and synthesized three derivatives of (SGT-405(2,7),¹⁸ SGT-410(2,7)

and **SGT-411**(2,7)¹⁹) via tuning the substitution position from the 2,7 to the 3,6 position of carbazole, which are coded as **SGT-405**(3,6), **SGT-410**(3,6) and **SGT-411**(3,6). It is worth to mention that the substitution position tuning from (2,7) to (3,6) position of carbazole moiety not only simplified synthesis routes (**Figure 2** and **Figure 3**), but also improved its hole transporting capability, which can be illustrated by its improved smooth film forming ability and hole mobility compared to **SGT-405**(2,7). With the device structure of FTO/compact TiO₂/meso-porous TiO₂/CH₃NH₃PbI_{3-x}Cl_x/HTM/Au, the **SGT-405**(3,6) showed a PCE of 18.87%, which is better than the photovoltaic devices based on *spiro-OMeTAD* (17.71%). To the best of our knowledge, the achieved PCE (18.87%) is the highest value reported for the devices with structure of FTO/compact TiO₂/meso-porous TiO₂/CH₃NH₃PbI_{3-x}Cl_x/HTM/Au employing small-molecular HTMs. Therefore, the simple synthesis and good performance of **SGT-405**(3,6) make it a very promising candidate for industrial production in the near future.

Results and discussion

The carbazole moiety consists of pyrrole ring fused to two benzene rings. The nitrogen in the pyrrole ring makes carbazole an electron-donating unit (p-type). Besides, the carbazole unit itself possesses good thermal stability, and further it can be functionalized with a variety of substituent to tune its thermal, photo-physical and electrochemical properties for OLED^{16,17,20} and solar cells.²¹ Therefore, carbazole derivatives have attracted much attention for organic semiconductors²²⁻²⁶ due to their good thermal stability, low-cost starting material, high electron-donating ability and chemical stability. In our previous work, carbazole derivatives based on the (2,7) substitution position of carbazole unit, **SGT-405**(2,7)¹⁸ and **SGT-411**(2,7)¹⁹ exhibited good photovoltaic performance when employed as HTMs for MAPbI₃-based perovskite solar cells. However, the preparation of 2,7-dibromocarbazole is a challenging task, which involves the nitration of 4,4'-dibromo biphenyl by nitric acid and cadogan reductive cyclization, as shown in **Figure 2**.²⁷⁻²⁹ Herein, we try to tune the substitution position from the 2,7 to 3,6 position of carbazole moiety, as shown in **Figure 2**. Compared to 2,7-dibromocarbazole, 3,6-dibromocarbazole is commercially available and cost-effective material. In addition, because the electron donating ability of the 3,6-carbazole is higher due to the fact that the N atom is at the para position in 3,6-carbazole derivatives,^{30, 31} we can expect that the newly designed 3,6-carbazole derivatives may have better hole transporting property. Therefore, we designed and synthesized new three carbazole derivatives, which are code as **SGT-405**(3,6), **SGT-410**(3,6) and **SGT-411**(3,6) (see **Figure 1**). The synthetic scheme for new designed molecules are shown in **Figure 3**.

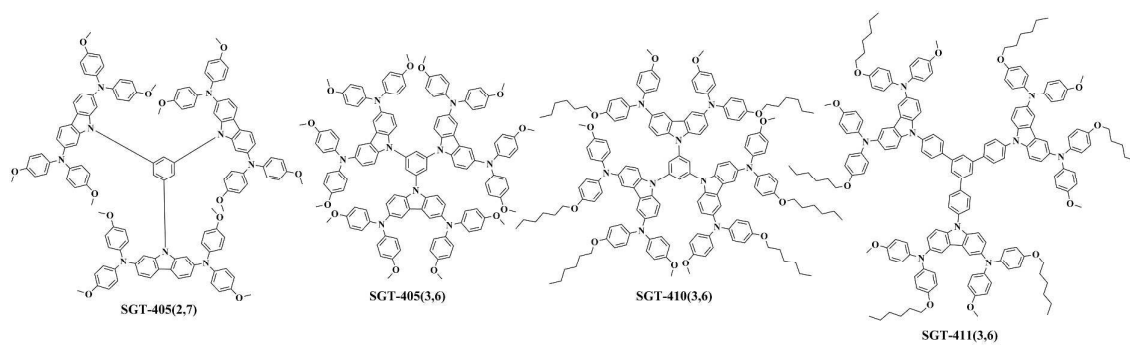


Figure 1. Molecular structures of SGT-405(3,6), SGT-410(3,6), SGT-411(3,6) and SGT-405(2,7).

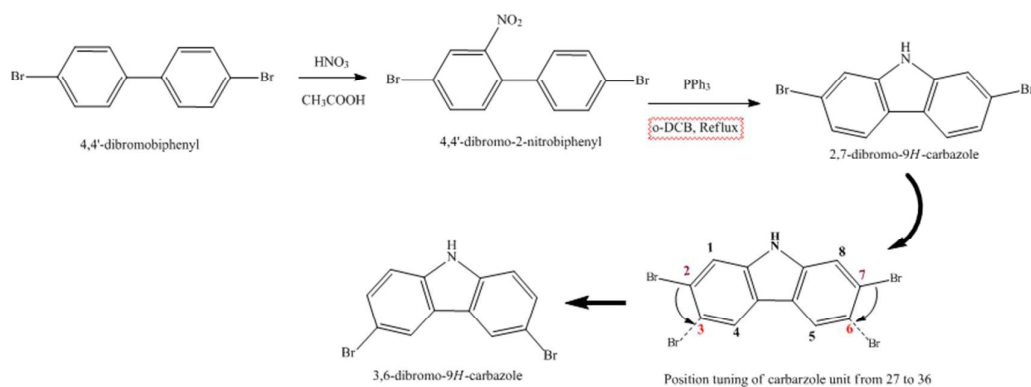


Figure 2. Synthetic diagram of substitution position tuning of carbazole moiety for low-cost carbazole-based small molecule HTMs for perovskite solar cells.

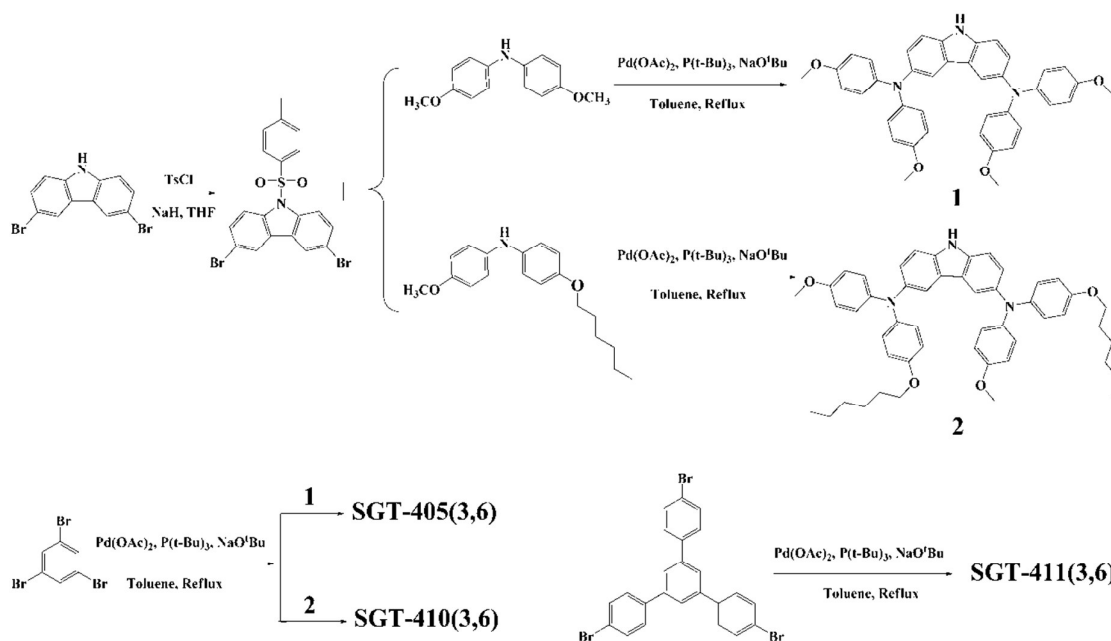


Figure 3. The synthetic routes for SGT-405(3,6), SGT-410(3,6) and SGT-411(3,6).

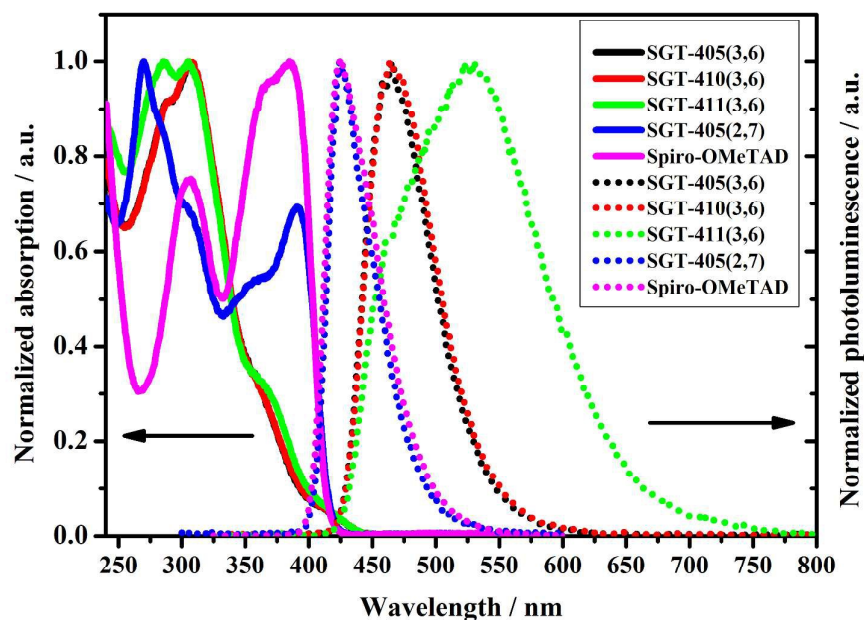


Figure 4. Normalized UV-Vis absorption and photoluminescence spectra of SGT-405(3,6), SGT-410(3,6), SGT-411(3,6) and reference HTMs (*spiro*-OMeTAD and SGT-405(2,7)) measured in DCM solution. (Note: The UV-Vis absorption spectra of SGT-405(3,6) coincide with that of SGT410(3,6)).

The normalized UV-vis absorption spectra of three new developed HTMs and reference HTMs (*spiro-OMeTAD* and **SGT-405(2,7)**) measured in dichloromethane are shown in **Figure 4**. The maximum absorption peaks of **SGT-405(3,6)**, **SGT-410(3,6)**, **SGT-411(3,6)** and reference molecules of *spiro-OMeTAD* and **SGT-405(2,7)** are summarized in **Table 1**. All new HTMs showed strong absorption bands at 270-310 nm, which are attributed to the π - π^* transitions of carbazole and **SGT** units, and weak absorption bands at 330-400 nm, corresponding to the n - π^* transitions of carbazole and **SGT** units.³² It is worth stating that no absorption peak of **SGT-405(3,6)**, **SGT-410(3,6)** and **SGT-411(3,6)** observed in visible region compared to *spiro-OMeTAD* is truly beneficial in terms of subduing the incident photon loss absorbed by the HTM layer itself.^{18, 33} Compared to the λ_{\max} of *spiro-OMeTAD* (385 nm), the λ_{\max} of **SGT-405(3,6)**, **SGT-410(3,6)** and **SGT-411(3,6)** are blue shifted to 306 nm, indicating that much weakened conjugation in **SGT-405(3,6)**, **SGT-410(3,6)** and **SGT-411(3,6)** than that of *spiro-OMeTAD*. The only chemical structure difference between **SGT-405(2,7)** and **SGT-405(3,6)** was shown in **Figure 1**. Even though the substitution position tuning from the (2,7) to the (3,6) of carbazole moiety leads to approximately 36 nm red shift of λ_{\max} , compared to **SGT-405(2,7)**, **SGT-405(3,6)** exhibits a much decreased absorption peak in the wavelength region of 350-425 nm. From the above absorption profiles, it could be confirmed that synthesized new HTMs can act as HTMs without interfering with the incident light absorbing process by perovskite layer.^{18, 34} The maximum emission peaks of **SGT-405(3,6)**, **SGT-410(3,6)** and **SGT-411(3,6)** are located at 466 nm, 466 nm and 530 nm, respectively. From the intersection of absorption and emission spectra, their band-gap can be estimated and summarized in **Table 1**.

The HOMO energy level was derived from the first oxidation potential, whereas the LUMO energy level was determined by subtracting the band-gap energy from the HOMO energy level. In order to determine the first oxidation potential (E_{ox}) of new developed HTMs, cyclic voltammetry (CV) experiments were conducted in DCM solution. The diagram of CV curves are shown in **Figure 5** and the corresponding energy levels are collected in **Table 1**. The HOMO energy level of *spiro-OMeTAD* measured is -5.25V, which is similar to the value of previous reported result.³⁵ The HOMO energy levels of new synthesized HTMs (-5.26 eV for **SGT-405(3,6)** and **SGT-410(3,6)**, -5.24 eV for **SGT-411(3,6)**) are very close to that of *spiro-OMeTAD* (-5.25 eV) and well aligned with the valence band of perovskite (-5.43 eV). The energy level alignment of the related materials used in this study are illustrated in **Figure 6**. The suitable HOMO energy levels of new developed HTMs allow holes to be extracted from perovskite to HTMs layer. In addition, LUMO energy levels of all new designed HTMs are much higher than the conduction band of perovskite, indicating that new designed HTMs could act as electron block layer and thus reduce the charge recombination processes.

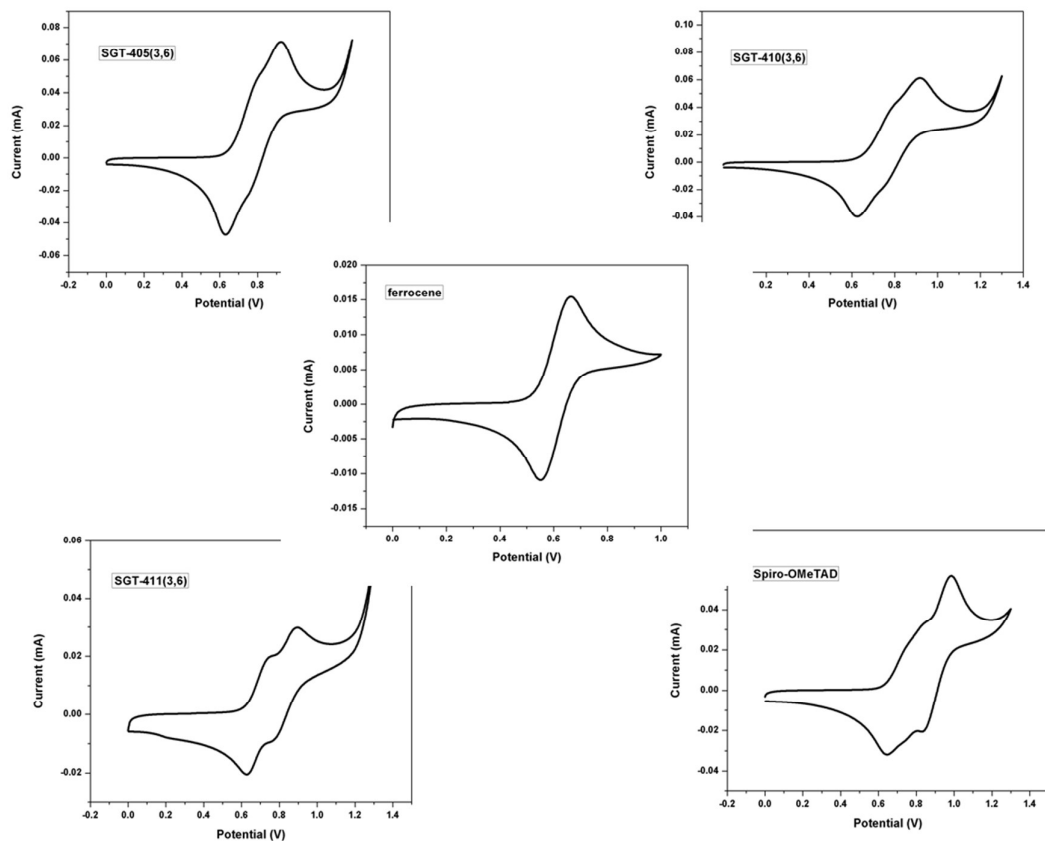


Figure 5. Cyclic voltammograms of **SGT-405(3,6)**, **SGT-410(3,6)**, **SGT-411(3,6)** and *spiro-OMeTAD* and the FC/FC⁺ redox couple in THF with 0.1 M tetra-*n*-butylammoniumhexafluorophosphate (TBAPF₆) as the supporting electrolyte with a scan rate of 50 mV S⁻¹.

Table 1. Photophysical and electrochemical properties of new HTMs, **SGT-405(2,7)** and *spiro-OMeTAD*.

| HTMs | λ_{abs} (nm) | ϵ ($\text{M}^{-1}\text{cm}^{-1}$) | λ_{em} (nm) | $E_{\text{ox}}^{\text{a)}$ (V vs NHE) | $E_{\text{gap}}^{\text{b)}$ (eV) | HOMO ^{c)} (eV) | LUMO ^{d)} (eV) | Hole Mobility ^{f)} ($\text{cm}^2\cdot\text{V}^{-1}\cdot\text{s}^{-1}$) | | | | | | | | | | | | | | | | | | | | | | | | | | | | | | | | | | | | | | | | | | | |
|---------------------|-----------------------------|---|-------------------------------|--|-------------------------------------|----------------------------|----------------------------|--|---------------------|-----|--------|-----|--------------------|------|-------|-------|----------------------|-----|--------|---------------------|-------|---------------------|-----|-------|------|-------|-------|----------------------|---------------------|----------------------|--------|-------|---------------------|--------------------|--------|-----|--------------------|------|-------|-------|----------------------|-------|-------|----------------------|-------|---------------------|-------|-------|-----|------|------|
| SGT-405(3,6) | 306 | 118070 | 466 | 0.76 | 2.92 | -5.26 | -2.34 | 1.8×10^{-4} | | | | | | | | | | | | | | | | | | | | | | | | | | | | | | | | | | | | | | | | | | | |
| | 360 | 35420 | | | | | | | SGT-410(3,6) | 306 | 117710 | 464 | 0.76 | 2.92 | -5.26 | -2.34 | 5.27×10^{-5} | 360 | 35310 | SGT-411(3,6) | 285 | 135630 | 530 | 0.74 | 2.91 | -5.24 | -2.33 | 8.74×10^{-5} | 306 | 135630 | 360 | 40690 | SGT-405(2,7) | 270 | 123480 | 424 | 0.75 ^{e)} | 3.03 | -5.25 | -2.22 | 1.05×10^{-4} | 358 | 64210 | 390 | 86440 | <i>spiro-OMeTAD</i> | 307 | 46800 | 425 | 0.75 | 3.05 |
| SGT-410(3,6) | 306 | 117710 | 464 | 0.76 | 2.92 | -5.26 | -2.34 | 5.27×10^{-5} | | | | | | | | | | | | | | | | | | | | | | | | | | | | | | | | | | | | | | | | | | | |
| | 360 | 35310 | | | | | | | SGT-411(3,6) | 285 | 135630 | 530 | 0.74 | 2.91 | -5.24 | -2.33 | 8.74×10^{-5} | 306 | 135630 | | 360 | 40690 | | | | | | | SGT-405(2,7) | 270 | 123480 | 424 | | 0.75 ^{e)} | 3.03 | | | | | | | -5.25 | -2.22 | 1.05×10^{-4} | 358 | | 64210 | 390 | | | |
| SGT-411(3,6) | 285 | 135630 | 530 | 0.74 | 2.91 | -5.24 | -2.33 | 8.74×10^{-5} | | | | | | | | | | | | | | | | | | | | | | | | | | | | | | | | | | | | | | | | | | | |
| | 306 | 135630 | | | | | | | | | | | | | | | | | | | | | | | | | | | | | | | | | | | | | | | | | | | | | | | | | |
| | 360 | 40690 | | | | | | | SGT-405(2,7) | 270 | 123480 | 424 | 0.75 ^{e)} | 3.03 | -5.25 | -2.22 | 1.05×10^{-4} | 358 | 64210 | 390 | 86440 | <i>spiro-OMeTAD</i> | 307 | 46800 | 425 | 0.75 | 3.05 | -5.25 | -2.20 | 8.32×10^{-5} | 366 | 58800 | 385 | 60000 | | | | | | | | | | | | | | | | | |
| SGT-405(2,7) | 270 | 123480 | 424 | 0.75 ^{e)} | 3.03 | -5.25 | -2.22 | 1.05×10^{-4} | | | | | | | | | | | | | | | | | | | | | | | | | | | | | | | | | | | | | | | | | | | |
| | 358 | 64210 | | | | | | | | | | | | | | | | | | | | | | | | | | | | | | | | | | | | | | | | | | | | | | | | | |
| | 390 | 86440 | | | | | | | <i>spiro-OMeTAD</i> | 307 | 46800 | 425 | 0.75 | 3.05 | -5.25 | -2.20 | 8.32×10^{-5} | 366 | 58800 | 385 | 60000 | | | | | | | | | | | | | | | | | | | | | | | | | | | | | | |
| <i>spiro-OMeTAD</i> | 307 | 46800 | 425 | 0.75 | 3.05 | -5.25 | -2.20 | 8.32×10^{-5} | | | | | | | | | | | | | | | | | | | | | | | | | | | | | | | | | | | | | | | | | | | |
| | 366 | 58800 | | | | | | | | | | | | | | | | | | | | | | | | | | | | | | | | | | | | | | | | | | | | | | | | | |
| | 385 | 60000 | | | | | | | | | | | | | | | | | | | | | | | | | | | | | | | | | | | | | | | | | | | | | | | | | |

a) Cyclic voltammograms measurements were carried out in THF solution with 0.1M TBAPF₆ as supporting electrolyte, ferrocene/ferrocenium($E(\text{Fc}/\text{Fc}^+) = 630 \text{ mV vs. NHE}$) as reference.

b) Calculated from the intersection of the normalized absorption and emission spectra measured in DCM solvent. (Figure 4).

c) $\text{HOMO} = -(E_{\text{ox}} + 4.5 \text{ eV})$.

d) $\text{LUMO} = \text{HOMO} + E_{\text{gap}}$.

e) E_{ox} of SGT-405(2,7) are collected from our published paper.¹⁸

f) Pure HTM without doping.

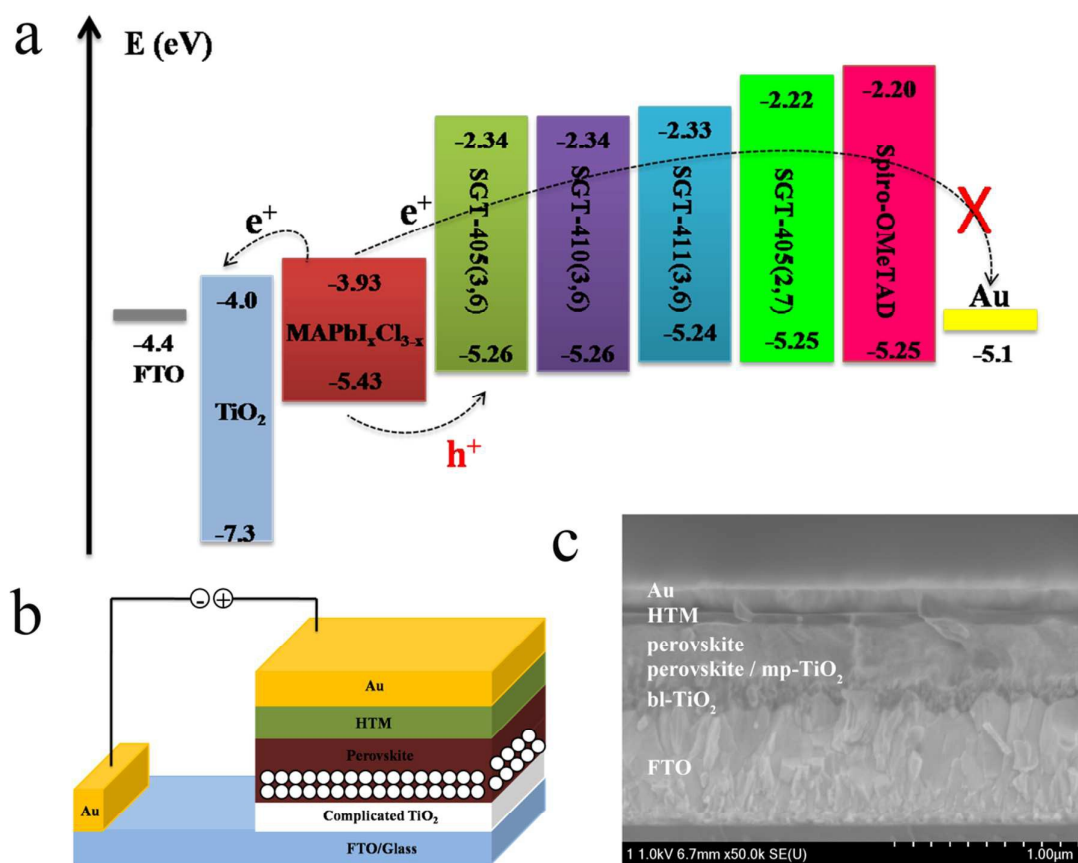


Figure 6. a) The energy level alignment of the related materials used in this study, b) Configuration of solar cell device used in this study, c) Cross-section of FE-SEM image of representative perovskite solar cells.

The thermal properties of various HTMs were studied by thermogravimetric analysis (TGA) and differential scanning calorimetry (DSC). The corresponding data are summarized in **Table 2**. And **Figure 7** shows that all of the new designed small molecules have high decomposition temperature (T_{dec}) located in the range of 372~400°C, with a weight loss of 5%, which is similar to that of *spiro-OMeTAD* (417°C), indicating newly developed HTMs possess good thermal stability. It is already reported that HTMs possessing higher glass transition temperature can reduce the tendency to orientated aggregation (crystallization) upon heating.^{36,37} The glass transition temperature (T_g) of HTMs is an important indicator for the morphology stability of amorphous film upon long time device storage or heating. Among them, **SGT-405(3,6)** exhibited very high glass transition (T_g) of 192.7°C (**Figure 8**). Comparison of T_g of **SGT-405(3,6)** with that of **SGT-405(2,7)** shows that substitution position tuning from (2,7) to (3,6) position of carbazole moiety leads to the increase of T_g by

44.1 °C. In addition, the glass transition temperature of **SGT-405(3,6)** is much higher than that of *spiro-OMeTAD* (125.8°C). However, there are no glass transition peaks detected for both **SGT-410(3,6)** and **SGT-411(3,6)**. Additionally, crystallization process is detected at 233°C for **SGT-405(3,6)** during first heating scan, whereas no crystallization was observed during the cooling and second and third heating step. In applying small molecular materials for electronic and optoelectronic devices, the morphology stability upon heating is often required, since phase transitions could take place during device operation (e.g., solar cells sitting continuously in direct sunlight can get quite hot, especially in hot climatic conditions). Therefore, we studied the morphology stability of various HTM films spin-coated onto glass substrate under different heating condition (w/o heating or heating at 130 °C for 1 hour) by polarized optical microscopy in atmosphere. When annealing treatment (130 °C, 1 hour) was applied on various HTM spin-coated films, enlarged crystallization areas were observed in the case of **SGT-405(2,7)**, **SGT-410(3,6)**, **SGT-411(3,6)** and *spiro-OMeTAD* films, while almost no change of surface morphology of **SGT-405(3,6)** was observed, indicating that **SGT-405(3,6)** exhibits the best morphology stability upon heating (stable amorphous) due to its very high T_g of 193 °C. (Figure S1).

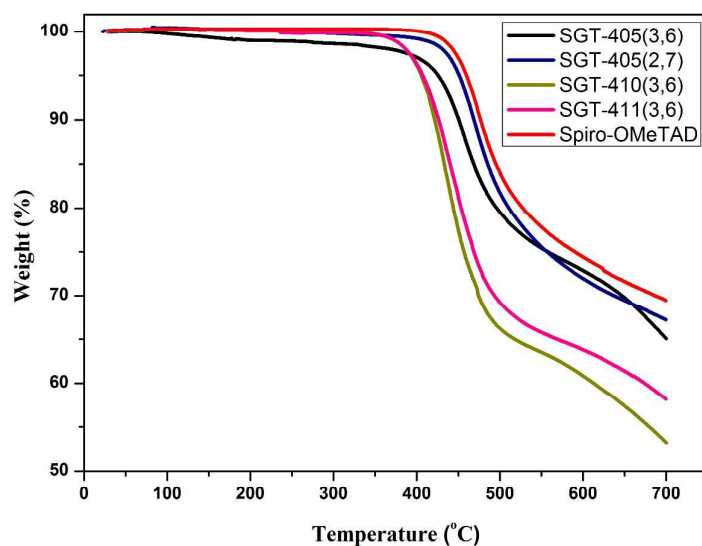


Figure 7. Thermogravimetric analysis data of **SGT-405(3,6)**, **SGT-410(3,6)**, **SGT-411(3,6)** and reference HTMs (*spiro-OMeTAD* and **SGT-405(2,7)**) with scan rate of 10°C min⁻¹ under N₂ atmosphere.

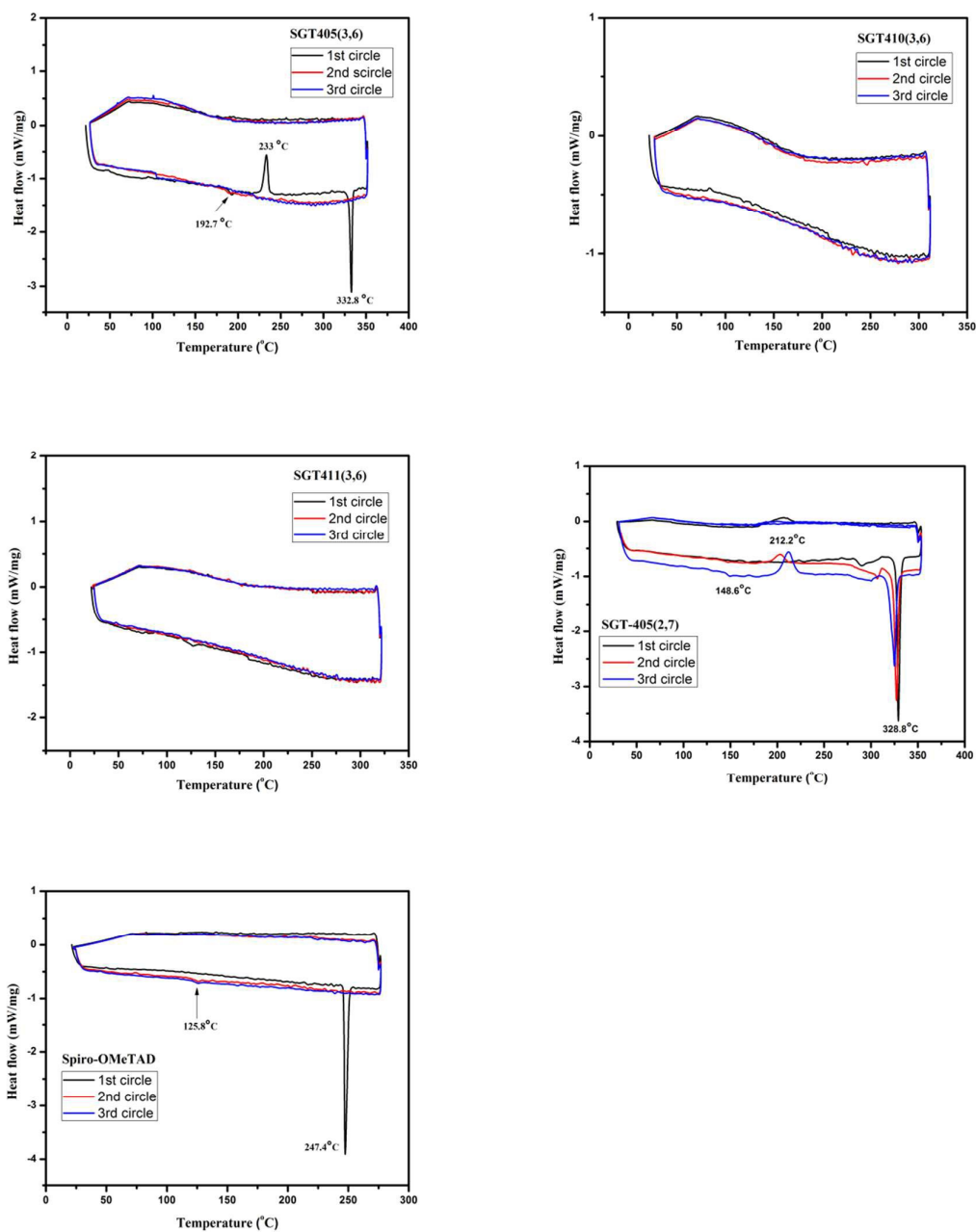


Figure 8. Differential scanning calorimetry traces of **SGT-405(3,6)**, **SGT-410(3,6)**, **SGT-411(3,6)** and other HTMs (*spiro-OMeTAD* and **SGT-405(2,7)**) with scan rate of $10^{\circ}\text{C min}^{-1}$ under N_2 atmosphere.

Table 2. Thermal properties of new developed HTMs and *spiro-OMeTAD*.

| HTMs | T _g (°C) ^{a)} | T _m (°C) ^{a)} | T _{cr} (°C) ^{a)} | T _{dec} (°C) ^{b)} |
|----------------------------|-----------------------------------|-----------------------------------|------------------------------------|-------------------------------------|
| SGT-405(3,6) | 192.7°C | 332.8°C | 233°C | 396°C |
| SGT-410(3,6) | - | - | - | 372°C |
| SGT-411(3,6) | - | - | - | 372°C |
| SGT-405(2,7) | 148.6°C | 328.8°C | 212.2 | 396°C |
| <i>spiro-OMeTAD</i> | 125.8°C | 247.4°C | - | 417°C |

a) Glass transition (collected from the second circle of DSC curve), melting and crystallization temperatures observed from DSC (10°Cmin⁻¹ under N₂ atmosphere)

b) Degradation temperature observed from TGA measurements (10°Cmin⁻¹ under N₂ atmosphere)

The uniformity of HTM capping layer spin-coated onto perovskite film was dramatically influenced by the solubility and aggregation behavior (related to the molecular structure) of HTMs.³⁸ It has been widely demonstrated that smooth film forming ability of HTM is very important for the creation of good interfacial contact of perovskite/HTM/Au, which could significantly affect the hole extraction and the charge recombination in device.^{39,40} Therefore surface morphology of various spin-coated HTMs film were investigated by FE-SEM. As shown in **Figure 9**, spin-coated **SGT-405(3,6)** film exhibits very smooth and uniform capping layer onto perovskite layer, which could be ascribed to its highly twisted non-planar molecular structure.⁴¹ As for spin-coated *spiro-OMeTAD* film, there are some nano-sized needle-shaped islands appeared as shown in **Figure 9f**, indicating that *spiro-OMeTAD* tends to oriented aggregation or crystallization due to its intrinsic feature,^{42,43} which is in agreement with the previous reported result that some very small crystals were observed in the spin-coated film of *spiro-OMeTAD*.⁴¹ The chemically structural difference of three new synthesized HTMs was shown in **Figure 1**. Long alkyl chains in **SGT-410(3,6)** and **SGT-411(3,6)** molecules were introduced to increase their solubility. However, a surprising phenomenon was observed, when compared to uniform **SGT-405(3,6)** film: Some sphere-shaped islands were observed in the spin-coated films of **SGT-410(3,6)** and **SGT-411(3,6)**, which could be ascribed to the aggregation induced by the additional van der Waals interactions stemming from the long alkyl chains.³⁸

In order to further study the top morphology of each HTM film spin-coated on top of perovskite layer, atomic forced microscopy was used to measure surface roughness of various HTM capping layers. As shown in **Figure 10**, the perovskite-only film without HTMs shows the largest surface roughness (RMS) of 15.989 nm (see **Figure 10a**), After the deposition of HTMs on top of perovskite films, the roughness was significantly decreased. The value of surface roughness decreases in the order of **SGT-411(3,6)**, *spiro-OMeTAD*, **SGT-410(3,6)**,

SGT-405(2,7) and **SGT-405(3,6)**. The 3D-AFM image of top morphology of **SGT-405(3,6)** (see **Figure 10b**) indicates that **SGT-405(3,6)** leads to the formation of uniform and full coverage capping layer on top perovskite film, which is agreed with the result from FE-SEM pictures, as shown in **Figure 9b**. It should be addressed that the surface morphology and roughness should have a strong influence on the photovoltaic performances. The relatively high fill factor of **SGT-405(3,6)** is partially contributed to its good film forming ability. The relatively low fill factor of **SGT-410(3,6)** and **SGT-411(3,6)** is partially ascribed to their roughness surface morphology.

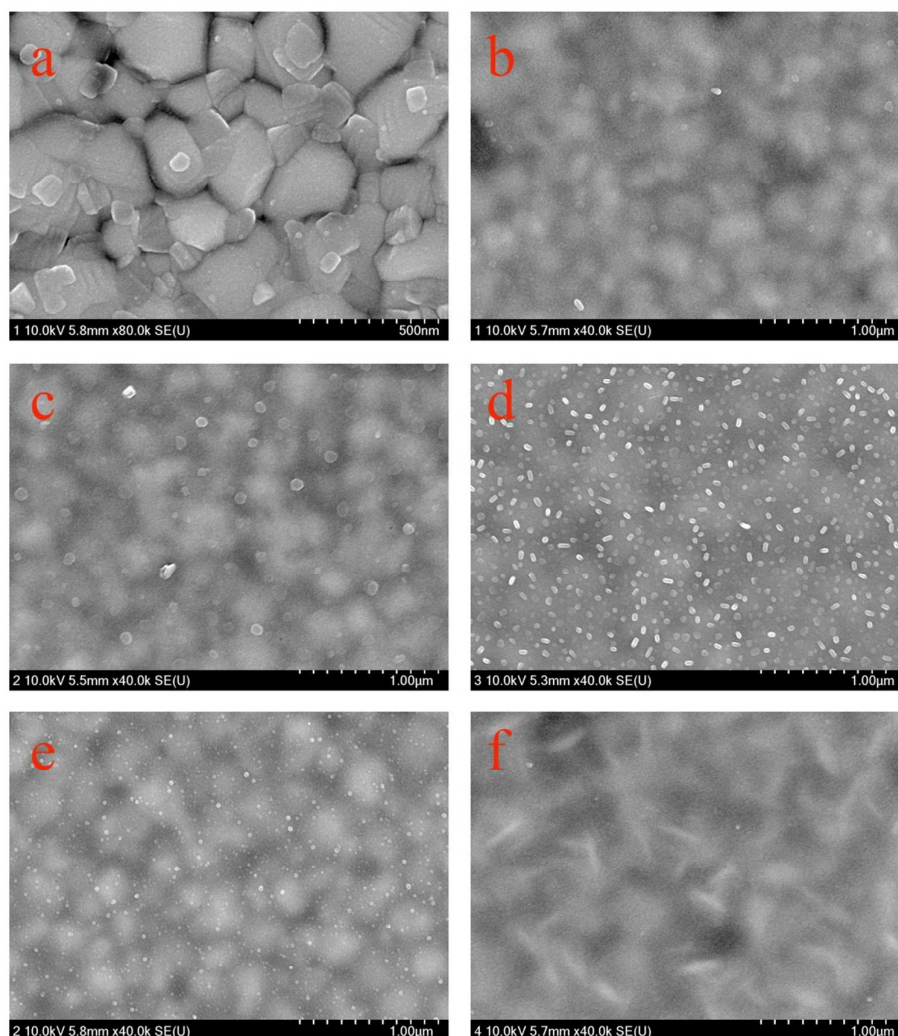


Figure 9. a) SEM- top view of the $\text{MAPbCl}_{3-x}\text{I}_x$ film. b-f) The top view of various HTM capping layers on the perovskite films; b) **SGT405(3,6)**; c) **SGT410(3,6)**; d) **SGT411(3,6)**; e) **SGT405(2,7)**; f) *spiro-OMeTAD*.

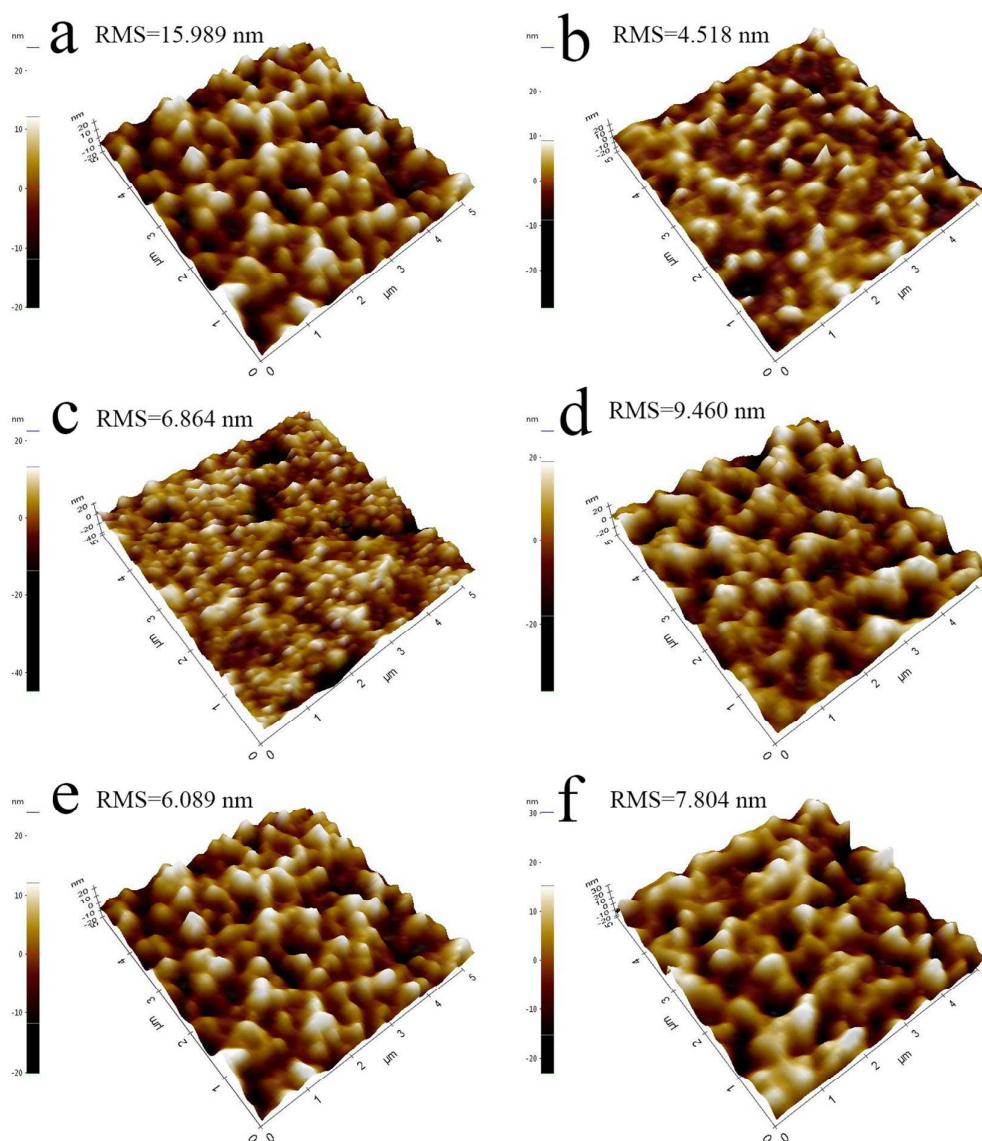


Figure 10. AFM images of top morphology of various films. a) MAPbCl_{3-x}I_x film; b-f) the top morphology of various HTM capping layers on the perovskite films: b) SGT405(3,6); c) SGT410(3,6); d) SGT411(3,6); e) SGT405(2,7); f) *spiro-OMeTAD*.

Hole mobility is another significant parameter to consider in the design of new HTMs for perovskite solar cells. Herein, the hole mobility of each new HTM synthesized was measured by using space-charge-limited current (SCLC) method.^{44, 45} The current density J_{sc} is limited by space charge and is given as:

$$J = \frac{9}{8} \mu \epsilon_0 \epsilon_r \frac{V^2}{d^3}$$

where J is the current density, μ is the hole mobility, ϵ_0 vacuum permittivity ($8.85 \times 10^{-12} \text{ F m}^{-1}$), ϵ_r is the dielectric constant of the material (normally taken to approach 3 for organic semiconductors)⁴⁶, V is the applied bias, and d is the film thickness. The hole only device structure used in this work: FTO/PEDOT:PSS/HTM/Au. Fitting the J-V curves (**Figure 11**) for each HTM applying to the equation evaluates the hole mobilities to be listed in **Table 1**. The value of hole mobility ($8.32 \times 10^{-5} \text{ cm}^2 \cdot \text{V}^{-1} \cdot \text{s}^{-1}$) of *spiro-OMeTAD* obtained here is very close to the value of $8.67 \times 10^{-5} \text{ cm}^2 \cdot \text{V}^{-1} \cdot \text{s}^{-1}$ reported in a previous literature.⁴⁷ As shown in **Table 1**, **SGT-410(3,6)** exhibits the lowest hole mobility ($5.27 \times 10^{-5} \text{ cm}^2 \cdot \text{V}^{-1} \cdot \text{s}^{-1}$). **SGT-405(3,6)** exhibits the highest hole mobility ($1.8 \times 10^{-4} \text{ cm}^2 \cdot \text{V}^{-1} \cdot \text{s}^{-1}$), followed by **SGT-405(2,7)** ($1.05 \times 10^{-4} \text{ cm}^2 \cdot \text{V}^{-1} \cdot \text{s}^{-1}$). **SGT-411(3,6)** shows comparable value of $8.74 \times 10^{-5} \text{ cm}^2 \cdot \text{V}^{-1} \cdot \text{s}^{-1}$ to that of *spiro-OMeTAD*.

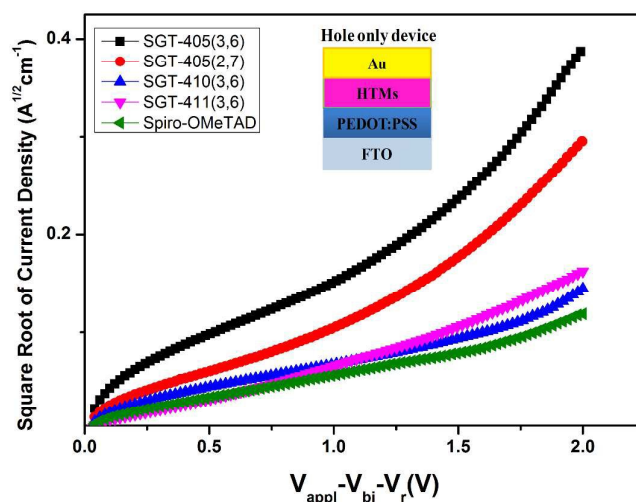


Figure 11. J-V characteristic of thin films in hole-only devices.

Space charge limited current (SCLC) measurements indicated that **SGT-405(3,6)** exhibited 1.8 times higher hole mobility than that of **SGT-405(2,7)**, but these two molecules show quite similar chemical structure to each other. To elucidate this from theoretical approach, density functional calculations were performed by using the B3LYP/6-31G(d,p) level with Gaussian 09 program. And *spiro-OMeTAD* used as a reference compound was calculated together using the same basis set and calculating method. The optimized geometry structures, detailed energy levels of frontier molecular orbitals and hole reorganization energy (λ) are summarized in **Figure 12**. The reorganization energy (λ) represents the relaxation of the molecule when one electron is withdraw or donated. Generally, based on the anatomy of a Marcus-type electron-transfer mechanism between the molecules, the small reorganization energy implies the fast transfer rate for electrons or holes to some extent.⁴⁵ As shown in

Figure 12, the hole reorganization energy of *spiro-OMeTAD* is 153.3 meV which is close to the value reported in previous literature.⁴⁵ The λ values of **SGT-405(3,6)** and **SGT-405(2,7)** molecules are 95 meV and 117.3 meV, respectively, indicating that **SGT405-(3,6)** exhibits a very small hole reorganization energy, much smaller than that of **SGT-405(2,7)** and *spiro-OMeTAD*, which agrees with the trend of hole mobility values measured by SCLC method. Furthermore, the λ value of 95 meV of **SGT-405(3,6)** is indeed comparable to the hole reorganization energies computed for the best organic p-type semiconducting materials (e.g., heteroacenes or oligoacenes).⁴⁸ These findings demonstrated that the substitution position tuning from (2,7) to (3,6) position of carbazole moiety not only simplified synthesis route, but also decreased its hole reorganization energy.

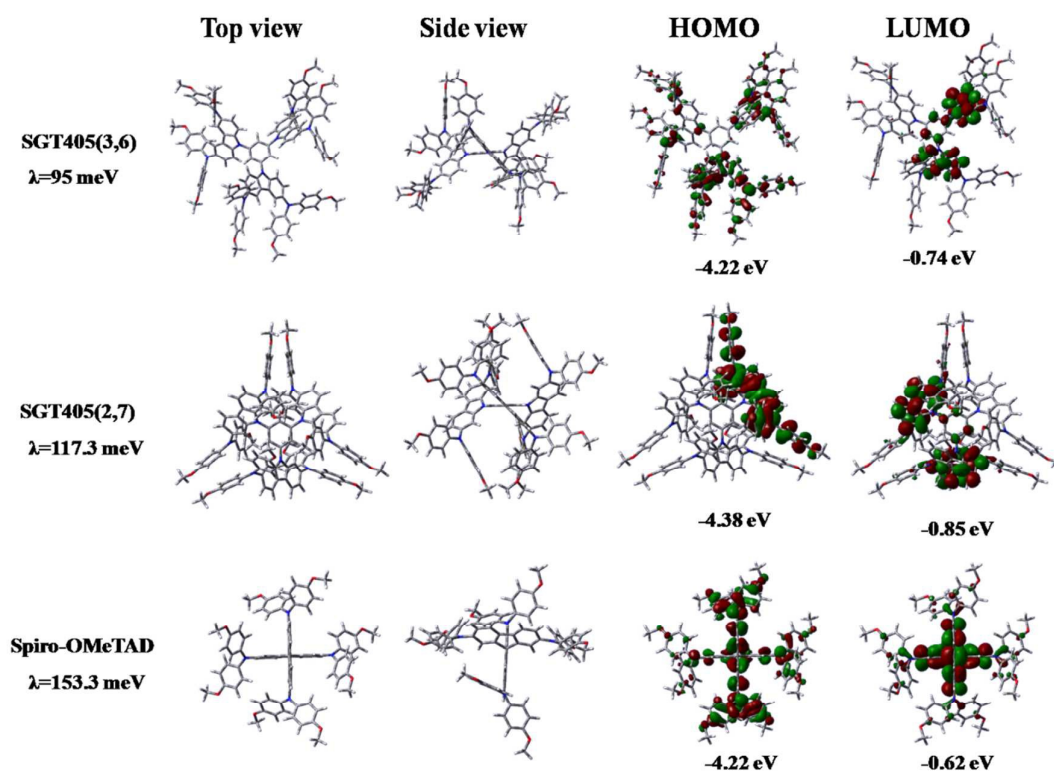


Figure 12. Results of DFT calculation (optimized molecular geometry, electron distributions of HOMO and LUMO energy levels and hole reorganization energy (λ) of **SGT405-(3,6)**, **SGT-405(2,7)** and *spiro-OMeTAD*).

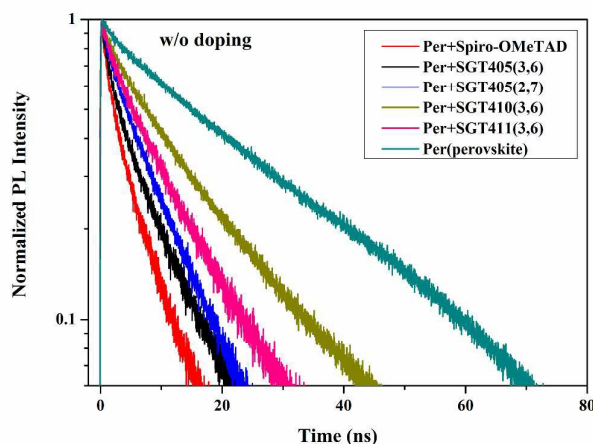


Figure 13. Time-resolved PL spectra of glass/perovskite and glass/perovskite/various HTMs measured at an excitation wavelength (393nm), and emission wavelength (750nm).

The interfacial hole transfer process between new HTM and perovskite can be investigated by TR-PL (time-resolved photoluminescence) measurements.³² **Figure 13** shows TR-PL spectra acquired from various perovskite films spin-coated with different HTMs. Compared with the neat perovskite films, the PL intensity is quenched much more significantly for *spiro-OMeTAD* and **SGT-405(3,6)**, followed by **SGT-405(2,7)**, **SGT-411(3,6)** and then **SGT-410(3,6)**, indicating that **SGT-405(3,6)** exhibits better hole extraction ability compared to that of **SGT-405(2,7)**, **SGT-411(3,6)** and **SGT-410(3,6)**.

From the characterization of newly synthesized HTMs by UV-Vis absorption and photoluminescence spectroscopy, cyclic voltammetry, thermogravimetric analysis, differential scanning calorimetry, scanning electron microscope, atomic force microscopy and space-charge-limited current (SCLC) measurement, we can expect that the newly developed HTMs have the potential to be applied as hole transporting materials for PrSCs. The high hole mobility of **SGT-405(3,6)** could potentially lead to high J_{sc} value for perovskite solar cells. Moreover, the high hole mobility and excellent film forming ability of **SGT-405(3,6)** could potentially lead to higher fill factor of the operating devices.³⁴

To evaluate the ability of synthesized compounds acting as HTM for PrSCs, the meso-porous type configuration of FTO/compact-TiO₂/mesoporous TiO₂/CH₃NH₃PbCl_{3-x}I_x/ HTM/Au in **Figure 6b** was used in this work. All devices were fabricated using one step deposition method with toluene dropping processes⁴⁹ and the detailed procedure is described in supporting information section. Different component layer of representative complete device can be seen clearly from the cross-section scanning electron microscopy (SEM) image in **Figure 6c**. For comparison, *spiro-OMeTAD* and **SGT-405(2,7)**¹⁸ were employed as reference HTMs in this study.

The J-V curves of perovskite solar cells with different HTMs were shown in **Figure 14a**. And their detailed parameters of photovoltaic performances were summarized in **Table 3**. *spiro-OMeTAD*-based device gives a PCE of 17.71% with J_{sc} of 22.01 mA/cm², FF of 76.58, V_{oc} of 1.051 V. **SGT-405(3,6)**-based PrSC device exhibits the highest PCE up to 18.87%, mainly coming from the enhanced J_{sc} of 22.93 mA/cm² and remarkable high FF of 78.65, while **SGT-405(2,7)**-based device exhibits a PCE of 18.0% with J_{sc} of 22.32 mA/cm², FF of 76.32, V_{oc} of 1.057 V. The FF is related to series resistance (R_s) and shunt resistance (R_{sh}). In order to obtain a high FF, the solar cells should have a low R_s and a high R_{sh} .⁵⁰ In other words, the HTM layer should effectively block the electron and transport the hole from MAPbCl_{3-x}I₃ to the Au electrode. The fabrication conditions used for all devices are the same, except for HTM. Therefore, the enhanced hole mobility and better film forming ability of **SGT-405(3,6)** compared to other HTMs used in this work, rendered **SGT-405(3,6)** based PrSC with enhanced J_{sc} of 22.928 mA/cm², remarkable high FF of 78.65 and the lowest R_s of 30.9Ω. The trend of fill factors of PrSCs device employing various HTMs followed a trend identical to the hole mobility of various HTMs, ascribed to a reduced R_s (series resistance). A straightforward method of estimating R_s for a solar cell is to calculate the slope of the J-V curve near V_{oc} .⁵¹ As shown in **Table 3**, **SGT-410(3,6)** and **SGT-411(3,6)** based PrSCs showed relatively high series resistance of 44.4 Ω and 45.2 Ω, respectively. **Figure 14b** shows the monochromatic incident photon conversion efficiency (IPCE) spectra of perovskite solar cells employing different HTMs, and the integrated photocurrent densities are in good agreement with the J_{sc} measured from J-V measurements.

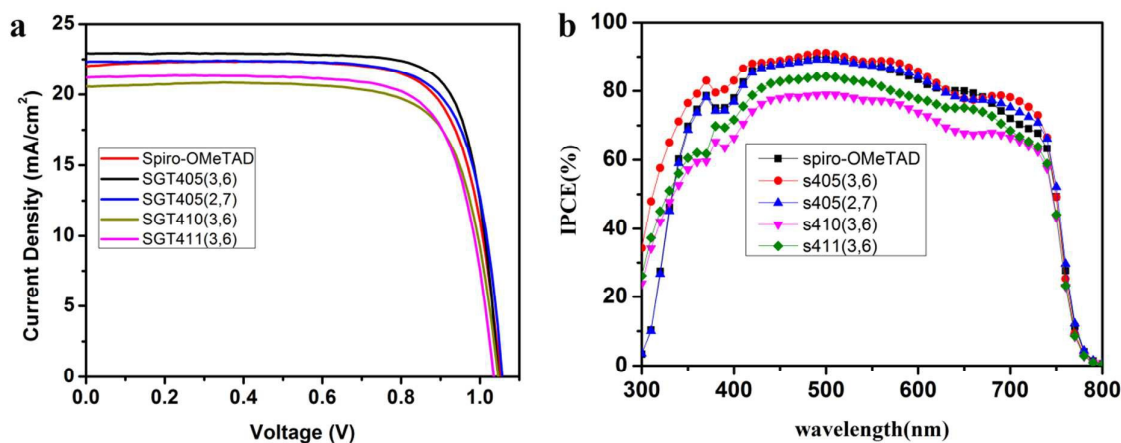
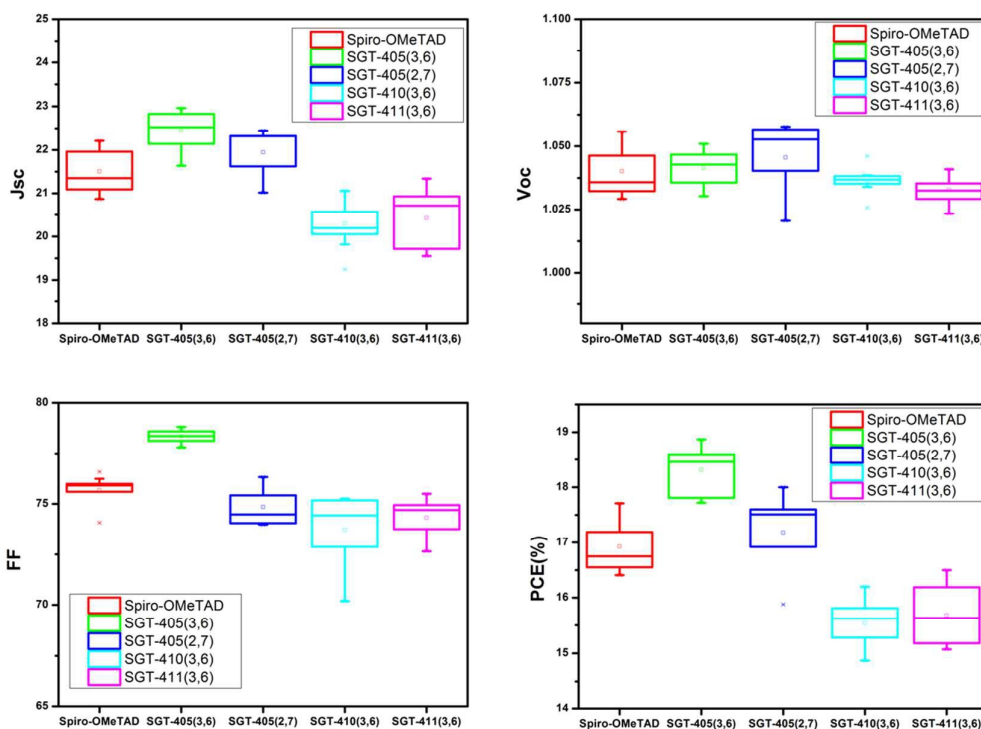


Figure 14. a) Current density (J)-voltage (V) curves of the best-performing solar cells with **SGT-405(3,6)**, **SGT-410(3,6)**, **SGT-411(3,6)**, **SGT-405(2,7)** and *spiro-OMeTAD* (measured under 100 mW·cm⁻²AM1.5G solar illumination); b) corresponding IPCE curves.

Table 3. Summary of photovoltaic parameters for the best-performing devices.

| HTMs | J_{sc} (mA/cm ²) | V_{oc} (V) | FF (%) | η (%) | Average η (%) | R_s (Ω) |
|---------------------|--------------------------------|--------------|--------|------------|--------------------|--------------------|
| SGT-405(3,6) | 22.928 | 1.0466 | 78.65 | 18.87 | 18.31±0.44 | 30.9 |
| SGT-410(3,6) | 20.574 | 1.0461 | 75.25 | 16.20 | 15.54±0.41 | 44.4 |
| SGT-411(3,6) | 21.190 | 1.0348 | 75.22 | 16.50 | 15.68±0.54 | 45.2 |
| SGT-405(2,7) | 22.321 | 1.0567 | 76.32 | 18.00 | 17.18±0.82 | 32.6 |
| spiro-OMeTAD | 22.009 | 1.0507 | 76.58 | 17.71 | 16.93±0.48 | 40.2 |

**Figure 15.** Device statistics of (a) J_{sc} , (b) V_{oc} , (c) fill factor and (d) PCE of the perovskite solar cells employing various HTMs.

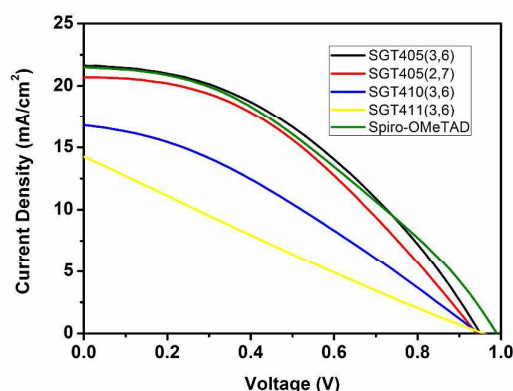


Figure 16. Current (J)–voltage (V) curves of the best-performing dopant-free solar cells employing various HTMs, **SGT405**-(3,6), **SGT-410**(3,6), **SGT-411**(3,6) and **SGT-405**(2,7) and *spiro-OMeTAD*.

Table 4. Summary of photovoltaic parameters for the best-performing dopant-free device using different developed HTMs.

| HTMs | J_{sc} (mA/cm ²) | V_{oc} (V) | FF (%) | η (%) | R_s (Ω) |
|----------------------|--------------------------------|--------------|--------|------------|--------------------|
| SGT-405 (3,6) | 21.625 | 0.9504 | 41.27 | 8.48 | 189 |
| SGT-410 (3,6) | 15.837 | 0.936 | 36.47 | 5.41 | 306 |
| SGT-411 (3,6) | 14.246 | 0.9581 | 23.64 | 3.23 | 865 |
| SGT-405 (2,7) | 20.699 | 0.9415 | 40.27 | 7.85 | 253 |
| <i>spiro-OMeTAD</i> | 21.519 | 0.99 | 38.16 | 8.13 | 202 |

To investigate the effect of HTMs on the cells stability, aging tests of the perovskite solar cells without encapsulation were performed under the same dark storage conditions (in atmosphere, at room temperature and the humidity in the range of 15% - 20%). As shown in **Figure 17**, **SGT-405**(3,6) exhibited the best device stability among five types of HTMs based PrSCs, while **SGT-411**(3,6) based devices rendered the poorest device stability. The device stability test results revealed that the improved stability of **SGT-405**(3,6)-based cell compared to other HTM-based devices could be attributed to the uniform HTM capping layer on the top of perovskite layer, preventing the moisture penetration into the perovskite layer.^{40, 43}

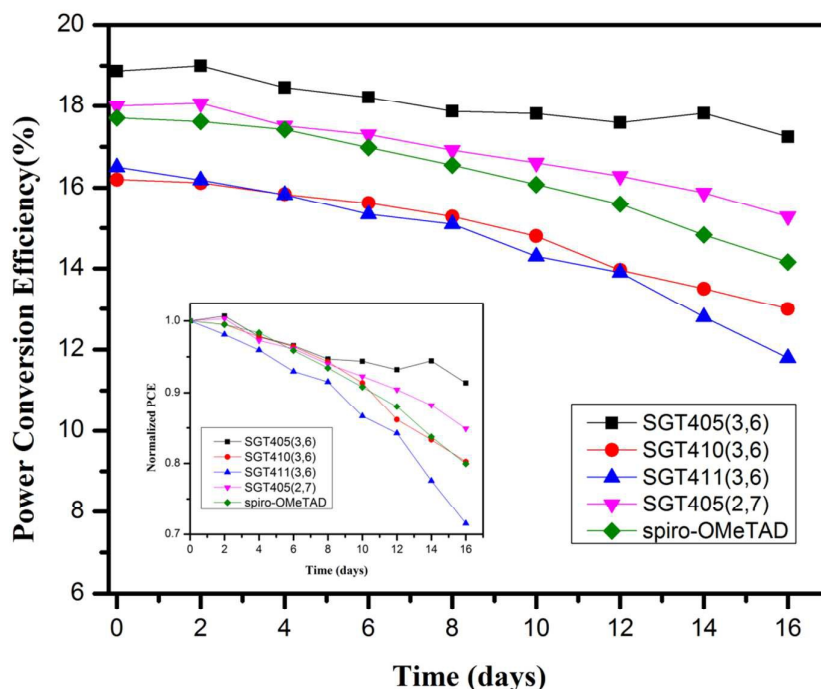


Figure 17. The long-term device stability tests for PrSC devices with various HTMs (in atmosphere, at room temperature and the humidity in the range of 15% - 20%). The inserted picture is the corresponding graph of normalized power conversion efficiency as function of time.

Cost evaluation

To compare the synthesis cost of **SGT-405(3,6)** with *spiro-OMeTAD* and **SGT-405(2,7)**, the lab synthesis cost of **SGT-405(3,6)** and **SGT-405(2,7)** were estimated by using the model proposed by Osedach et al.⁵² More detail information about the synthesis cost is available in supporting information section.

Table 5. Comparison of the estimated material costs.

| HTMs | Material cost ((€/g) ^[a] | Commercial price((€/g) |
|-----------------------------------|-------------------------------------|------------------------|
| SGT-405(3,6) | 29.65 | - |
| SGT-405(2,7)^[b] | 88.08 | - |
| <i>spiro-OMeTAD</i> | 96.09 ^[c] | 186-580 |

[a] Material cost estimated for the synthesis of 1 g of product.

[b] Synthetic scheme taken from our published paper.¹⁸

[c] Taken from the reference.⁵³

Conclusions

In this study, three new carbazole-based starburst small molecule HTMs, which are coded as **SGT-405(3,6)**, **SGT-410(3,6)** and **SGT-411(3,6)**, were designed and synthesized on the basis of our previous work^{18, 19} via tuning the substitution position from (2,7) to (3,6) position of carbazole moiety. This makes them easily synthesized via three-step from commercially available starting materials. They were characterized by UV-Vis absorption and photoluminescence spectroscopy, cyclic voltammetry, scanning electron microscope and atomic force microscopy and space charge limited current (SCLC) measurement. Among them, **SGT-405(3,6)** exhibits high glass transition temperature (192.7°C), good solubility, excellent film forming ability and high hole mobility compared to *spiro-OMeTAD*. Meanwhile **SGT-405(3,6)** shows very small hole reorganization energy (95 meV). These analytic results demonstrate that the substitution position tuning from (2,7) to (3,6) position of carbazole moiety not only simplified synthesis route, but also improved its hole transporting performance, which can be illustrated by its improved smooth film forming ability, reduced hole reorganization energy (λ) and increased hole mobility compared to **SGT-405(2,7)**. Owing to the promising characteristics of **SGT-405(3,6)**, with the device structure of FTO/compact TiO₂/meso-porous TiO₂/CH₃NH₃PbI_{3-x}Cl_x/HTM/Au, the device employing **SGT-405(3,6)** as HTM affords a remarkable conversion efficiency of 18.87%, which is better than that of *spiro-OMeTAD* based device (17.71%) under the same fabrication conditions. To the best of our knowledge, the achieved PCE (18.87%) is the highest conversion efficiency among the device with structure of FTO/compact TiO₂/meso-porous TiO₂/CH₃NH₃PbI_{3-x}Cl_x/HTM/Au employing small-molecular HTMs. In addition, the long-term device stability of PrSCs was enhanced for **SGT-405(3,6)** compared to other HTMs studied here due to the good uniform capping layer of **SGT-405(3,6)** on top of perovskite layer and the prevention of the moisture penetration into the perovskite layer. Our work demonstrates **SGT-405(3,6)** is a promising alternative non-spiro type small molecular HTM with low-cost and excellent performance for existing cost ineffective and synthetically-challenging *spiro-OMeTAD* in perovskite solar cells.

Acknowledgements

This work was supported by the National Research Foundation of Korea (NRF) grant funded by the Korean government (MSIP) through the Mid-career Researcher Program (2014R1A2A1A10051630) as well as Climate Change Program (2015M1A2A2056543) and the Functional Districts of the Science Belt Support Program, Ministry of Science, ICT and Future Planning (2015K000287).

References

1. M. M. Lee, J. Teuscher, T. Miyasaka, T. N. Murakami and H. J. Snaith, *Science*, 2012, **338**, 643-647.
2. J. S. Manser, M. I. Saidaminov, J. A. Christians, O. M. Bakr and P. V. Kamat, *Accounts of Chemical Research*, 2016, **49**, 330-338.
3. C. Wehrenfennig, G. E. Eperon, M. B. Johnston, H. J. Snaith and L. M. Herz, *Advanced Materials*, 2014, **26**, 1584-1589.
4. G. Xing, N. Mathews, S. Sun, S. S. Lim, Y. M. Lam, M. Grätzel, S. Mhaisalkar and T. C. Sum, *Science*, 2013, **342**, 344-347.
5. S. D. Stranks, G. E. Eperon, G. Grancini, C. Menelaou, M. J. P. Alcocer, T. Leijtens, L. M. Herz, A. Petrozza and H. J. Snaith, *Science*, 2013, **342**, 341-344.
6. V. D'Innocenzo, G. Grancini, M. J. P. Alcocer, A. R. S. Kandada, S. D. Stranks, M. M. Lee, G. Lanzani, H. J. Snaith and A. Petrozza, *Nature Communications*, 2014, **5**, 3586.
7. C. Zuo, H. J. Bolink, H. Han, J. Huang, D. Cahen and L. Ding, *Advanced Science*, 2016, **3**, n/a-n/a.
8. NREL, Best Research-Cell Efficiencies, <https://www.nrel.gov/pv/assets/images/efficiency-chart.png>, (accessed April, 2017).
9. W. E. Forum, the top 10 emerging technologies of 2016, <https://www.weforum.org/agenda/2016/06/top-10-emerging-technologies-2016/>.
10. L. Calió, S. Kazim, M. Grätzel and S. Ahmad, *Angewandte Chemie International Edition*, 2016, **55**, 14522-14545.
11. T. P. I. Saragi, T. Spehr, A. Siebert, T. Fuhrmann-Lieker and J. Salbeck, *Chemical Reviews*, 2007, **107**, 1011-1065.
12. K. Rakstys, M. Saliba, P. Gao, P. Gratia, E. Kamarauskas, S. Paek, V. Jankauskas and M. K. Nazeeruddin, *Angewandte Chemie International Edition*, 2016, **55**, 7464-7468.
13. A. W. Schmidt, K. R. Reddy and H.-J. Knölker, *Chemical Reviews*, 2012, **112**,

- 3193-3328.
14. G. Puckyte, B. Schmaltz, A. Tomkeviciene, M. Degbia, J. V. Grazulevicius, H. Melhem, J. Bouclé and F. Tran-Van, *Journal of Power Sources*, 2013, **233**, 86-92.
 15. N. Prachumrak, S. Pojanasopa, S. Namuangruk, T. Kaewin, S. Jungsuttiwong, T. Sudyoasuk and V. Promarak, *ACS Applied Materials & Interfaces*, 2013, **5**, 8694-8703.
 16. K. L. Paik, N. S. Baek, H. K. Kim, J.-H. Lee and Y. Lee, *Macromolecules*, 2002, **35**, 6782-6791.
 17. S.-H. Jung, H. K. Kim, S.-H. Kim, Y. H. Kim, S. C. Jeoung and D. Kim, *Macromolecules*, 2000, **33**, 9277-9288.
 18. S. D. Sung, M. S. Kang, I. T. Choi, H. M. Kim, H. Kim, M. Hong, H. K. Kim and W. I. Lee, *Chemical Communications*, 2014, **50**, 14161-14163.
 19. M. S. Kang, S. D. Sung, I. T. Choi, H. Kim, M. Hong, J. Kim, W. I. Lee and H. K. Kim, *ACS Applied Materials & Interfaces*, 2015, **7**, 22213-22217.
 20. P. Kundu, K. R. Justin Thomas, J. T. Lin, Y. T. Tao and C. H. Chien, *Advanced Functional Materials*, 2003, **13**, 445-452.
 21. N. Blouin, A. Michaud and M. Leclerc, *Advanced Materials*, 2007, **19**, 2295-2300.
 22. G. Sathiyar, E. K. T. Sivakumar, R. Ganesamoorthy, R. Thangamuthu and P. Sakthivel, *Tetrahedron Letters*, 2016, **57**, 243-252.
 23. J. Li and A. C. Grimsdale, *Chemical Society Reviews*, 2010, **39**, 2399-2410.
 24. P. Li, H. Tong, J. Ding, Z. Xie and L. Wang, *Journal of Materials Chemistry A*, 2013, **1**, 8805-8812.
 25. S. H. Park, A. Roy, S. Beaupre, S. Cho, N. Coates, J. S. Moon, D. Moses, M. Leclerc, K. Lee and A. J. Heeger, *Nat Photon*, 2009, **3**, 297-302.
 26. N. Blouin, A. Michaud, D. Gendron, S. Wakim, E. Blair, R. Neagu-Plesu, M. Belletête, G. Durocher, Y. Tao and M. Leclerc, *Journal of the American Chemical Society*, 2008, **130**, 732-742.
 27. A. W. Freeman, M. Urvoy and M. E. Criswell, *The Journal of Organic Chemistry*, 2005, **70**, 5014-5019.
 28. R. Singh, J. S. Meena, C.-S. Wu and F.-H. Ko, *Physical Chemistry Chemical Physics*, 2015, **17**, 5227-5235.
 29. X. Liu, Y. Sun, Y. Zhang, F. Miao, G. Wang, H. Zhao, X. Yu, H. Liu and W.-Y. Wong, *Organic & Biomolecular Chemistry*, 2011, **9**, 3615-3618.
 30. H. Wang, G. Chen, X. Xu, H. Chen and S. Ji, *Dyes and Pigments*, 2010, **86**, 238-248.
 31. S.-M. Park, K.-S. Yook, W.-H. Lee, Y. Hong, J.-Y. Lee and I.-N. Kang, *Journal of Polymer Science Part A: Polymer Chemistry*, 2013, **51**, 5111-5117.
 32. K. Rakstys, A. Abate, M. I. Dar, P. Gao, V. Jankauskas, G. Jacopin, E. Kamarauskas, S. Kazim, S. Ahmad, M. Grätzel and M. K. Nazeeruddin, *Journal of the American*

- Chemical Society*, 2015, **137**, 16172-16178.
33. Y.-K. Wang, Z.-C. Yuan, G.-Z. Shi, Y.-X. Li, Q. Li, F. Hui, B.-Q. Sun, Z.-Q. Jiang and L.-S. Liao, *Advanced Functional Materials*, 2016, **26**, 1375-1381.
34. A. Molina-Ontoria, I. Zimmermann, I. Garcia-Benito, P. Gratia, C. Roldán-Carmona, S. Aghazada, M. Graetzel, M. K. Nazeeruddin and N. Martín, *Angewandte Chemie International Edition*, 2016, **55**, 6270-6274.
35. H.-S. Kim, C.-R. Lee, J.-H. Im, K.-B. Lee, T. Moehl, A. Marchioro, S.-J. Moon, R. Humphry-Baker, J.-H. Yum, J. E. Moser, M. Graetzel and N.-G. Park, *Sci. Rep.*, 2012, **2**.
36. X. Zhao, S. Wang, J. You, Y. Zhang and X. Li, *Journal of Materials Chemistry C*, 2015, **3**, 11377-11384.
37. T. Malinauskas, D. Tomkute-Luksiene, R. Sens, M. Daskeviciene, R. Send, H. Wonneberger, V. Jankauskas, I. Bruder and V. Getautis, *ACS Applied Materials & Interfaces*, 2015, **7**, 11107-11116.
38. I. Zimmermann, J. Urieta-Mora, P. Gratia, J. Aragón, G. Grancini, A. Molina-Ontoria, E. Ortí, N. Martín and M. K. Nazeeruddin, *Advanced Energy Materials*, 2016, DOI: 10.1002/aenm.201601674, n/a-n/a.
39. J. Zhang, B. Xu, M. B. Johansson, M. Hadadian, J. P. Correa Baena, P. Liu, Y. Hua, N. Vlachopoulos, E. M. J. Johansson, G. Boschloo, L. Sun and A. Hagfeldt, *Advanced Energy Materials*, 2016, **6**, n/a-n/a.
40. J. Zhang, B. Xu, M. B. Johansson, N. Vlachopoulos, G. Boschloo, L. Sun, E. M. J. Johansson and A. Hagfeldt, *ACS Nano*, 2016, **10**, 6816-6825.
41. B. Xu, J. Zhang, Y. Hua, P. Liu, L. Wang, C. Ruan, Y. Li, G. Boschloo, E. M. J. Johansson, L. Kloo, A. Hagfeldt, A. K. Y. Jen and L. Sun, *Chem*, 2017, **2**, 676-687.
42. T. Qin, W. Huang, J.-E. Kim, D. Vak, C. Forsyth, C. R. McNeill and Y.-B. Cheng, *Nano Energy*, 2017, **31**, 210-217.
43. M. Li, Z.-K. Wang, Y.-G. Yang, Y. Hu, S.-L. Feng, J.-M. Wang, X.-Y. Gao and L.-S. Liao, *Advanced Energy Materials*, 2016, **6**, n/a-n/a.
44. T. Leijtens, I. K. Ding, T. Giovenzana, J. T. Bloking, M. D. McGehee and A. Sellinger, *ACS Nano*, 2012, **6**, 1455-1462.
45. B. Xu, H. Tian, L. Lin, D. Qian, H. Chen, J. Zhang, N. Vlachopoulos, G. Boschloo, Y. Luo, F. Zhang, A. Hagfeldt and L. Sun, *Advanced Energy Materials*, 2015, **5**, n/a-n/a.
46. H. J. Snaith and M. Grätzel, *Applied Physics Letters*, 2006, **89**, 262114.
47. B. Xu, E. Sheibani, P. Liu, J. Zhang, H. Tian, N. Vlachopoulos, G. Boschloo, L. Kloo, A. Hagfeldt and L. Sun, *Advanced Materials*, 2014, **26**, 6629-6634.
48. A. N. Sokolov, S. Atahan-Evrenk, R. Mondal, H. B. Akkerman, R. S. Sánchez-Carrera, S. Granados-Focil, J. Schrier, S. C. B. Mannsfeld, A. P. Zoombelt, Z. Bao and A. Aspuru-Guzik, 2011, **2**, 437.

49. N. J. Jeon, J. H. Noh, Y. C. Kim, W. S. Yang, S. Ryu and S. I. Seok, *Nat Mater*, 2014, **13**, 897-903.
50. N. J. Jeon, J. Lee, J. H. Noh, M. K. Nazeeruddin, M. Grätzel and S. I. Seok, *Journal of the American Chemical Society*, 2013, **135**, 19087-19090.
51. N. J. Jeon, H. G. Lee, Y. C. Kim, J. Seo, J. H. Noh, J. Lee and S. I. Seok, *Journal of the American Chemical Society*, 2014, **136**, 7837-7840.
52. T. P. Osedach, T. L. Andrew and V. Bulovic, *Energy & Environmental Science*, 2013, **6**, 711-718.
53. M. L. Petrus, T. Bein, T. J. Dingemans and P. Docampo, *Journal of Materials Chemistry A*, 2015, **3**, 12159-12162.

Graphic abstract

Simple Synthesis and Molecular Engineering of Low-cost and Star-shaped Carbazole-based Hole Transporting Materials for Highly Efficient Perovskite Solar Cells

Chunyuan Lu^a, In Taek Choi^a, Jeongho Kim^b and Hwan Kyu Kim^{a,*}

^aGlobal GET-Future Lab. and Department of Advanced Materials Chemistry, Korea University, Sejong 300-79, Korea

^bDepartment of Chemistry, Inha University, 100 Inha-ro, Incheon 402-751, Korea

